

# Charge order in LuFe<sub>2</sub>O<sub>4</sub>: antiferroelectric ground state and coupling to magnetism

M. Angst,<sup>1,2,\*</sup> R. P. Hermann,<sup>2,3</sup> A. D. Christianson,<sup>4</sup> M. D. Lumsden,<sup>4</sup> C. Lee,<sup>5</sup> M.-H. Whangbo,<sup>5</sup>  
J.-W. Kim,<sup>6</sup> P. J. Ryan,<sup>6</sup> S. E. Nagler,<sup>4</sup> W. Tian,<sup>1,6</sup> R. Jin,<sup>1</sup> B. C. Sales,<sup>1</sup> and D. Mandrus<sup>1</sup>

<sup>1</sup>*Materials Science and Technology Division, Oak Ridge National Laboratory, Oak Ridge, TN 37831, USA*

<sup>2</sup>*Institut für Festkörperforschung, Forschungszentrum Jülich GmbH, D-52425 Jülich, Germany*

<sup>3</sup>*Department of Physics, B5, Université de Liège, B-4000 Sart-Tilman, Belgium*

<sup>4</sup>*Neutron Scattering Science Division, Oak Ridge National Laboratory, Oak Ridge, TN 37831, USA*

<sup>5</sup>*Department of Chemistry, North Carolina State University, Raleigh, NC 27695, USA*

<sup>6</sup>*Ames Laboratory, Ames, IA 50010, USA*

(Dated: November 2, 2018)

X-ray scattering by multiferroic LuFe<sub>2</sub>O<sub>4</sub> is reported. Below 320 K, superstructure reflections indicate an incommensurate charge order with propagation close to  $(\frac{1}{3}\frac{1}{3}\frac{3}{2})$ . The corresponding charge configuration, also found by electronic structure calculations as most stable, contains polar Fe/O double-layers with *antiferroelectric* stacking. Diffuse scattering at 360 K, with  $(\frac{1}{3}\frac{1}{3}0)$  propagation, indicates ferroelectric short-range correlations between neighboring double-layers. The temperature dependence of the incommensuration indicates that charge order and magnetism are coupled.

PACS numbers: 71.30.+h, 77.80.-e, 75.80.+q, 61.05.C-

Materials where ferroelectricity or dielectric behavior is coupled to magnetism have the potential for novel applications and presently receive a lot of attention [1]. A new type of ferroelectricity, originating from charge order (CO) and seemingly coupled to magnetism, has been proposed to occur in LuFe<sub>2</sub>O<sub>4</sub> containing triangular Fe/O double-layers [2], generating a lot of interest in this material [3, 4, 5, 6, 7, 8]. Ferroelectricity is thought to arise from a particular arrangement of Fe<sup>2+</sup> and Fe<sup>3+</sup> within the Fe/O double-layers, making these intrinsically polar. However, different reported [8, 9] superstructure reflections indicate an incomplete understanding of the CO, and the full three-dimensional (3D) charge configuration has yet to be established. The latter determines the stacking of the polarizations of the individual double-layers, and thus the net polarization of the material.

Further, although magnetism in LuFe<sub>2</sub>O<sub>4</sub> occurs in the CO state to date there is no direct observation of coupling between CO and magnetism to date. Such an observation would be important in establishing the mechanism by which ferroelectricity, dielectric behavior, and magnetism couple via the underlying CO. We have recently grown LuFe<sub>2</sub>O<sub>4</sub> crystals with magnetic transitions of unprecedented sharpness, on which neutron scattering allowed the first refinement of a 3D spin structure [10].

Here, we present a study of the CO superstructure by synchrotron x-ray scattering. We propose a commensurate approximation for three domains of the incommensurate CO configuration, with propagations (in hexagonal notation) close to the symmetry-equivalent directions  $(\frac{1}{3}\frac{1}{3}\frac{3}{2})$ ,  $(\frac{2}{3}\frac{1}{3}\frac{3}{2})$ , and  $(\frac{1}{3}\frac{2}{3}\frac{3}{2})$ , corresponding to an *antiferroelectric* [11] ground state that we also identify by first-principles density-functional theory (DFT) as having the lowest energy. In contrast, short-range charge correlations above the CO temperature were found to correspond to a ferroelectric CO configuration

with  $(\frac{1}{3}\frac{1}{3}0)$  propagation. Further, we provide evidence for a coupling between CO and magnetism involving primarily the incommensuration of the CO. Our results underline the importance of near degeneracy of the CO in LuFe<sub>2</sub>O<sub>4</sub> and provide an essential microscopic basis for magnetoelectric coupling previously proposed [2, 3, 4, 5].

We studied single crystals from the same batch as those in [10]. X-ray scattering was performed on the (001) surface of a crystal with a mosaic of 0.02(1)° at beam line 6IDB of the Advanced Photon Source, using 16.2 keV photons. All scattered intensities are normalized to an ion chamber monitor. Structural Bragg reflections, denoted  $\mathbf{s}$ , are consistent with the reported [12] rhombohedral  $R\bar{3}m$  structure. Specific heat was measured with commercial equipment.

Superstructure reflections (Fig. 1) appear below a sharp feature in the specific heat (inset) at  $T_{CO} \sim 320$  K indicating the CO transition [13]. We found two sets of strong superstructure reflections at the same  $hkl$  positions as reported in [9], one set near  $(\frac{1}{3}\frac{1}{3}\frac{o}{2})$  with  $o$  an odd integer, and satellites to  $(00\frac{3o}{2})$  at  $\pm(\tau\tau 0)$  and (not previously reported) two symmetry-equivalent directions [ $\tau \sim 0.03$ , see Fig. 2(a)]. As proposed in [9], the positions of these reflections are consistent with three CO domains (labelled A, B, and C hereafter) with the symmetry-equivalent propagation vectors  $\mathbf{p}_A = (\frac{1}{3} + \delta, \frac{1}{3} + \delta, \frac{3}{2})$ ,  $\mathbf{p}_B = (\frac{2}{3} - 2\delta, \frac{1}{3} + \delta, \frac{3}{2})$ , and  $\mathbf{p}_C = (\frac{1}{3} + \delta, \frac{2}{3} - 2\delta, \frac{3}{2})$ . Here,  $\delta \sim 0.003$  is very small, but  $\delta \neq 0$  implies *incommensurate* CO. The reflections near  $(\frac{1}{3}\frac{1}{3}\frac{o}{2})$  correspond to  $\mathbf{s} \pm \mathbf{p}_i$ , and several additional, much weaker, types of reflections visible in Fig. 1 have positions consistent with  $\mathbf{s} \pm n\mathbf{p}_i$ , to be discussed in detail elsewhere. The reflections shown in Fig. 2 may be considered as higher harmonics as well, likely  $\mathbf{s} \pm 9\mathbf{p}_i$  ( $\tau = 9\delta$ ), and are in any case a consequence of a bimodal charge distribution of the CO configuration obtained below.

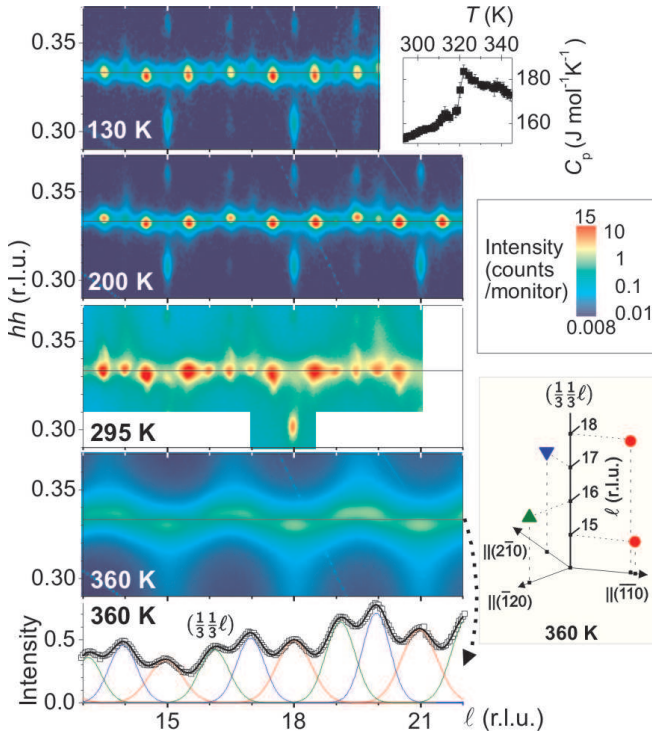


FIG. 1: (Color online) Scattered intensity at  $(hhl)$  at 130, 200, 295, and 360 K. Lowest panel:  $(\frac{1}{3}\frac{1}{3}\ell)$  cut at 360 K with fit by Gaussians. Strong structural reflections reach intensities  $> 10^4$  counts/monitor, strong superstructure reflections  $\sim 40$ . The higher overall intensity at 295 K is due to wider detector slits being used. Horizontal lines mark  $hh = \frac{1}{3}$ . Insets: Specific heat near 320 K; sketch of  $hkl$  positions of maxima in diffuse scattering at 360 K, with symbols indicating domains as in Fig. 3(a).

To estimate domain populations we collected x-ray diffraction data on a second crystal [14], using a  $\text{CuK}\alpha$  diffractometer [Fig. 3(a,b)]. Intensities of superstructure reflections close to  $(\frac{1}{3}\frac{1}{3}\frac{o}{2})$  and equivalent directions are shown in Fig. 3(a). Reflections at positions  $\mathbf{s} \pm \mathbf{p}_A$ ,  $\mathbf{s} \pm \mathbf{p}_B$ , and  $\mathbf{s} \pm \mathbf{p}_C$  are indicated by  $\blacksquare$ ,  $\blacktriangle$ , and  $\blacktriangledown$ , respectively. Taking into account that  $R\bar{3}m$  structural reflections occur only for  $-h+k+l=3n$  with  $n$  integer, each observed superstructure reflection is associated with one particular domain. All measurements are consistent with domain A being almost unpopulated, and domain B roughly twice more populated than domain C. The intensity ratios of satellite pairs around  $(0,0,19.5)$  [Fig. 3(b)], each pair arising from one domain, indicate the same domain populations, supporting the hypothesis that they are resulting from the same CO configuration. The consistent domain populations obtained from the intensities confirms the  $\mathbf{p}_A$ ,  $\mathbf{p}_B$ ,  $\mathbf{p}_C$ , propagation type proposed above.

To determine the CO configurations corresponding to propagations  $\mathbf{p}_A$ ,  $\mathbf{p}_B$ , and  $\mathbf{p}_C$ , we performed representation analysis [15, 16]. Similar to the spin order determined earlier [10], there are two allowed irreducible CO

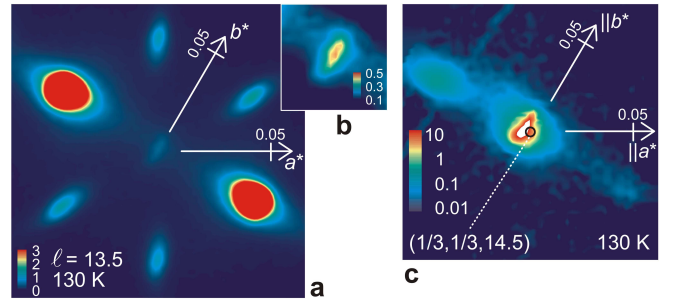


FIG. 2: (Color online) Incommensurate satellites. (a) Intensity at  $(hk13.5)$  at 130 K (the two strongest peaks reach  $\sim 19$  counts/mon). (b) Detail around  $(0,0,13.5)$ . (c) Intensity around  $(\frac{1}{3}\frac{1}{3}14.5)$  (marked by  $\circ$ ).

representations i) and ii), corresponding to either same or different valence for the 1 and 2 Fe sites [Fig. 3(c,d)] of the primitive cell. For simplicity, our following discussion assumes a commensurate approximation ( $\delta, \tau \rightarrow 0$ ) [18] in which the propagation vectors become  $(\frac{1}{3}\frac{1}{3}\frac{3}{2})$  and symmetry-equivalent wavevectors. Both representations contain sites with two different magnitudes of the Fe valence difference from average, in clear contrast to the results of Mössbauer spectroscopy, which imply a bimodal valence distribution [17]. A bimodal charge distribution is only obtained by adding a uniquely defined  $(00\frac{3}{2})$  representation. Case i) leads to a CO configuration in which the Fe/O double-layers are not charge neutral. This is physically very unlikely, given the separation of neighboring double-layers by  $\sim 6$  Å. Case ii) leads to a single feasible configuration with overall neutral double-layers, see Fig. 3(c). Shown is the configuration for domain A, accommodated in a  $\sqrt{3} \times \sqrt{3} \times 2$  supercell. Note that the CO lowers [19] the crystallographic space group symmetry to monoclinic  $C2/m$ . For this CO configuration, structure factor calculations [20] confirm the observed reflection pattern, including both  $\mathbf{s} \pm \mathbf{p}$  and  $\mathbf{s} \pm (00\frac{3}{2})$ . The latter, in the commensurate approximation, correspond to the reflections shown in Fig. 2(a), again confirming the association of both these types of reflections with the same CO. As a further check of the proposed CO [Fig. 3(c)], we used this solution to re-analyze the 220 K neutron data presented in [10]. Combining the CO model with the previous model of spin order, magnetic scattering at both  $(\frac{1}{3}\frac{1}{3}n)$  and  $(\frac{1}{3}\frac{1}{3}\frac{o}{2})$  could be refined successfully [21].

For the above CO model, the configuration in each individual double-layer is polar as proposed in [2]. However, the stacking of the polarization of the six double layers of the supercell [Fig. 3(c)] is antiferroelectric with no net polarization. To confirm this antiferroelectric configuration, we carried out DFT calculations for the ferrielectric and antiferroelectric CO within a  $\sqrt{3} \times \sqrt{3} \times 2$  cell (in addition to the  $\sqrt{3} \times \sqrt{3} \times 1$  calculations of [6]), that indeed show that the antiferroelectric CO configuration is

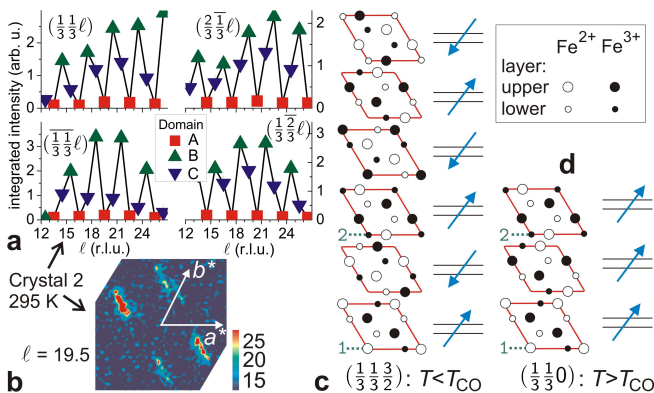


FIG. 3: (Color online) Commensurate approximation of the charge configuration. (a) Integrated intensities of  $(\frac{1}{3}\frac{1}{3}\frac{0}{2})$  type reflections. Reflections associated with different domains are indicated by different symbols (see text). (b) scattered intensity at  $(hk19.5)$ . (c,d) Charge configuration for domain A for  $T < T_{CO}$  (c) and  $T > T_{CO}$  (d, short-range). Shown are the Fe ions (see legend) of the 6  $(3)$  Fe/O double-layers of the  $\sqrt{3}\times\sqrt{3}\times 2$  ( $\times 1$ ) supercell. The direction of the local polarization for each double layer is indicated by an arrow. The two sites of the primitive cell are numbered (see text).

more stable than the ferrielectric one [by 3.2 meV/fu (formula unit)], and hence corresponds to the ground state.

Our result raises the question how the remanent polarization indicated by pyroelectric current measurements [2] could be explained. A simple explanation would be that the samples are different, since the strong oxygen stoichiometry-dependence of physical properties is well-known. However, this is unlikely to apply, for two reasons. First, superstructure reflections published in the same paper as the polarization results [2] and other papers by the same group (e.g., [9]), are consistent with  $(\frac{1}{3}\frac{1}{3}\frac{3}{2})$  propagation. Our structure factor calculations indicate that all CO configurations with non-zero net polarization have  $(\frac{1}{3}\frac{1}{3}n)$  reflections of the same order of magnitude as  $(\frac{1}{3}\frac{1}{3}\frac{0}{2})$  reflections, whereas no  $(\frac{1}{3}\frac{1}{3}n)$  reflections are reported in [2, 9]. Second, preliminary pyroelectric current measurements with a similar protocol as in [2] suggest a similar remanent polarization as in [2].

Before presenting an alternative explanation, we turn to the diffuse scattering observed above  $T_{CO}$ . Heating through  $T_{CO}$ , the  $(\frac{1}{3}\frac{1}{3}\frac{0}{2})$  and all satellite reflections weaken [Fig. 4(c,d)], as expected, but  $(\frac{1}{3}\frac{1}{3}n)$  reflections *gain* in intensity [Fig. 4(b)]. At 360 K there is still considerable diffuse scattering present around the  $(\frac{1}{3}\frac{1}{3}\frac{0}{2})$  rod, see Fig. 1. A cut in  $hhl$  along  $(\frac{1}{3}\frac{1}{3}\frac{0}{2})$  reveals broad maxima now at *integer*  $\ell$  positions, well described by strongly overlapping Gaussians (lowest panel). The positions of these diffuse peaks are sketched in an inset to Fig. 1. They are consistent with  $(\frac{1}{3} - \delta', \frac{1}{3} - \delta', 0)$  propagation and equivalent. The width of the Gaussians in Fig. 1 indicates that CO correlations in  $c$  direction ( $\xi_c$ ) extend to 2–3 double-layers [22], i.e. they are 3D rather than 2D,

in contrast to [9]. Representation analysis for the above propagation again yielded two irreducible representations [23], one rejected as unphysical due to non-charge-neutral double-layers. The remaining representation in commensurate approximation leads to a CO configuration [Fig. 3(d)] with  $\sqrt{3}\times\sqrt{3}\times 1$  cell and ferroelectric stacking of the polarization of the double-layers. Our DFT calculations using the  $\sqrt{3}\times\sqrt{3}\times 2$  cell show that this ferroelectric configuration is less stable than the antiferroelectric configuration (i.e., the ground state), but only by 13.4 meV/fu or 3% of the overall CO gain.

Although with  $\xi_c \lesssim c$  the description in terms of CO configurations may seem somewhat questionable, the result suggests that the high  $T$  correlations favor a ferroelectric arrangement between neighboring double-layers. It is thus surprising that, upon long-range charge ordering, the configuration established is not ferroelectric. Given the small energy-differences between antiferro- and ferroelectric configurations it seems likely that cooling with an electric field applied may stabilize long-range order of the ferroelectric CO configuration, which would explain the remanent polarization observed (only) after cooling in an electric field. This idea should be tested by scattering experiments with electric fields applied in-situ.

In zero electric field, the ground-state has the same *basic* CO configuration with no net polarization at all  $T$  below  $T_{CO}$ , but specific features vary with  $T$ . Here, we focus on the temperature dependence of the incommensuration of the CO. As in  $\text{Fe}_2\text{OBO}_3$  [24], the incommensuration  $\tau$  [25] changes with  $T$  [Fig. 4(e)], but in  $\text{LuFe}_2\text{O}_4$  it is much smaller and present at all  $T$ . In the fluctuation regime,  $\tau$  decreases rapidly upon cooling below  $T_{CO}$ , suggesting that the incommensuration may be an important factor in stabilizing either ferro- or antiferroelectric CO. This trend is reversed at  $T_N \sim 240$  K, where  $\tau \sim 0.025$  has a minimum: The appearance of the seemingly commensurate [10] magnetic order results in forcing the CO to become more incommensurate. In the center of the satellite rings [Fig. 2(a,b)], weak additional reflections develop upon cooling through  $T_N$  [Fig. 4(a)]. The emergence of these additional reflections is not completely understood at present, but provides an additional indication of coupling between the CO and the magnetism.

At the low  $T$  transition  $T_{LT} \sim 175$  K reported in [10] the width and intensity of these additional reflections change, and a moderate impact on various other reflections and  $\tau(T)$  is readily visible in Fig. 4. While a detailed discussion of the impact of the low  $T$  transition on CO and other degrees of freedom is beyond the scope of this work, we like to point out that i) the basic CO configuration remains the same upon cooling through  $T_{LT}$ , and ii) the CO correlation along  $c$  is slightly ( $\sim 7\%$ ) improved compared to 200 K, suggesting a better established CO. In contrast, the magnetic order is less established below  $T_{LT}$  as indicated by the broadness of various magnetic reflections and diffuse magnetic component re-

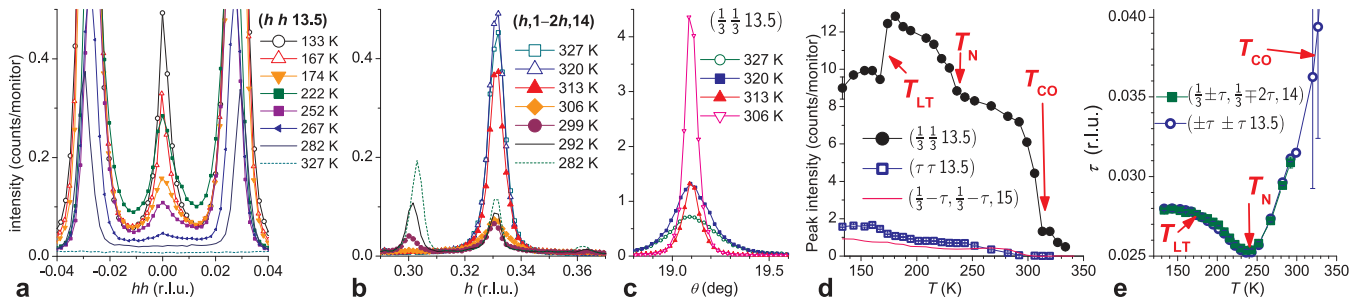


FIG. 4: (Color online)  $T$  dependence of CO on warming. (a)  $(hh13.5)$  scans. (b) Scans  $\parallel(1\bar{2}0)$  through  $(\frac{1}{3}\frac{1}{3}14)$ . (c)  $(\frac{1}{3}\frac{1}{3}13.5)$  rocking curves. (d) Peak intensities of three reflections vs  $T$ . (e) Incommensuration  $\tau(T)$ .

ported in [10]. Thus the “final compromise” between CO and magnetism, established below  $T_{LT}$  on approaching the ground state, seems more favorable to the CO.

In conclusion, we show by scattering experiments and DFT calculations that the charge-ordered polar Fe/O double-layers of LuFe<sub>2</sub>O<sub>4</sub> have antiferroelectric stacking in the ground state. Upon long-range ordering, the high- $T$  ferroelectric short-range correlations revert to this stacking. The incommensurate nature of the resulting CO is likely relevant for stabilizing either ferro- or antiferroelectric charge configurations, and reveals the coupling of the CO to the magnetism, a coupling likely related to the observed [3] large magneto-dielectric effect.

We thank D. S. Robinson for assistance and J. Voigt, H. J. Xiang, H. M. Christen, W. Schweika, A. Kreyssig, Y. Janssen, S. Nandi, and A. B. Harris for discussions. Work at ORNL, NCSU, and at the MU-CAT sector of APS was supported by the Division of Materials Sciences and Engineering, Office of Basic Energy Sciences, US Department of Energy (DE-AC05-00OR22725, DE-FG02-86ER45259, DE-ACD2-07CH11358, and DE-AC02-06CH11357).

\* Electronic address: m.angst@fz-juelich.de

- [1] W. Eerenstein, N. D. Mathur, and J. F. Scott, *Nature* **442**, 759 (2006); S.-W. Cheong and M. Mostovoy, *Nat. Mater.* **6**, 13 (2007); M. Bibes and A. Barthélemy, *ibid.* **7**, 425 (2008).
- [2] N. Ikeda *et al.*, *Nature* **436**, 1136 (2005).
- [3] M. A. Subramanian *et al.*, *Adv. Mater.* **18**, 1737 (2006).
- [4] A. Nagano *et al.*, *Phys. Rev. Lett.* **99**, 217202 (2007); M. Naka, A. Nagano, and S. Ishihara, *Phys. Rev. B* **77**, 224441 (2008).
- [5] J. Y. Park *et al.*, *Appl. Phys. Lett.* **91**, 152903 (2007).
- [6] H. J. Xiang and M.-H. Whangbo, *Phys. Rev. Lett.* **98**, 246403 (2007).
- [7] C.-H. Li *et al.*, *Appl. Phys. Lett.* **92**, 182903 (2008).

- [8] Y. Zhang *et al.*, *Phys. Rev. Lett.* **98**, 247602 (2007).
- [9] Y. Yamada *et al.*, *Phys. Rev. B* **62**, 12167 (2000); J. Phys. Soc. Jpn. **66**, 3733 (1997).
- [10] A. D. Christianson *et al.*, *Phys. Rev. Lett.* **100**, 107601 (2008).
- [11] We use the term only to indicate the nature of polar arrangements, not implying reversal of polar arrangements in electric fields, though this seems likely [2] as well.
- [12] M. Isobe *et al.*, *Acta Cryst. C* **46**, 1917 (1990).
- [13] A freezing of charge hopping is confirmed by optical and Mössbauer spectroscopies [17].
- [14] The second crystal was untwinned. In contrast, the first crystal contains the common defect “180°-twinning” [Y. Zhang *et al.*, *Phys. Rev. B* **76**, 184105 (2007)], that led to structural reflections with either  $-h+k+l=3n$  or  $h-k+l=3n$ , preventing an intensity analysis.
- [15] A. S. Wills, *Physica B* **276**, 680 (2000); <http://www.chem.ucl.ac.uk/people/wills>.
- [16] W. Sikora, F. Bialas, and L. Pytlik, *J. Appl. Cryst.* **37**, 1015 (2004); <http://www.ftj.agh.edu.pl/~sikora/modyopis.htm>.
- [17] X. S. Xu *et al.*, arXiv:0809.4483 (unpublished).
- [18] This likely describes the CO locally [see, e.g., [24]] and using the incommensuration in the representation analysis does not lead to an overall polarization either.
- [19] The crystallographic symmetry follows the CO symmetry due to atom shifts accompanying the CO. See, e.g., M. Angst *et al.*, *Phys. Rev. Lett.* **99**, 086403 (2007).
- [20] As described by N. Ikeda, S. Mori, and K. Kohn, *Ferroelectrics* **314**, 41 (2005).
- [21] Though with an unexpectedly high magnetic contrast between Fe ions in the two valence states. Details will be given elsewhere.
- [22] This is a lower limit, because the cut does not go through the peak maxima. Cutting at  $(\frac{1}{3}\frac{1}{3}\ell)$  is the best “compromise” (compare with the sketch in Fig. 1).
- [23] Here, addition of a (000) component is necessary to obtain a bimodal charge distribution.
- [24] M. Angst *et al.*, *Phys. Rev. Lett.* **99**, 256402 (2007).
- [25] Our discussion of the temperature dependence of the incommensuration is based on  $\tau$  rather than  $\delta$  because the latter is too small to be accurately measured, and  $\tau \propto \delta$ .